Absolute Calibration of the OMEGA Streaked Optical Pyrometer for Laser-Driven Shock Waves

Introduction

Equation-of-state (EOS) physics at extreme pressures and temperatures is important in inertial confinement fusion (ICF),[1,2] astrophysics,[3] material sciences,[4] and other areas of high-energy-density physics (HEDP).[5,6] Of particular importance is the relation of a material's thermal-state variables to its mechanical-state variables. A typical EOS study entails an impedance-matching experiment to determine the kinematic properties (pressure, density, and internal energy) of a material coupled with a simultaneous temperature measurement to provide its thermal behavior (temperature and entropy).[7] Laser-driven shock-wave experiments produce extremely high pressures and enable one to measure a material's behavior at extreme conditions ($P > 1$ Mbar; $T > 1$ eV) (Ref. 8). The Omega Laser Facility[9] readily produces these conditions over nanosecond time scales and millimeter-scale areas. Diagnosis of these experiments requires relatively high spatial and temporal resolution. A line-imaging velocity interferometer system for any reflector (VISAR)[10] is used to determine the material's mechanical-state variables by measuring shock velocities with ~50-ps and <10-μm resolution. A streaked optical pyrometer (SOP) simultaneously records the space/time history of the material's thermal self-emission between 590 and 850 nm with similar temporal and spatial resolution.[10] Self-emission from the shock-compressed material is converted to a brightness temperature by comparing its emission to that of a black-body radiator.[11] Together these measurements provide temperature as a function of pressure or density.

By absolutely calibrating the SOP over its wavelength range, one is able to measure the spectral radiance of an emitting shock front and assign it a brightness temperature. This article presents the technique and results of the absolute calibration of the OMEGA SOP. The details of recent design changes to the SOP, upgraded in 2011, are also presented.

Experimental Configuration

In a typical laser-driven shock-wave experiment, a target is irradiated by lasers (direct drive) or by x rays from a laser-driven hohlraum (indirect drive).[1] These drivers cause the outer layer of the target (the ablator) to blow off and expand outward, launching a forward-moving shock wave through the target material. The shock compresses the material and induces high temperature, pressure, and internal energy.

Opposite the drive beams, the reflected VISAR probe beam and the self-emission from the shock are collected by an *f*/3.3 telescope. As shown in Fig. 138.23(a), the telescope, mounted on a mechanical stage, consists of a two-lens objective (L1/L2) followed by a planoconvex singlet (L3). The combined signal (reflected probe and self-emission) first encounters the meniscus lens (L1) that also acts as a disposable blast shield that prevents debris from hitting the next optic, a collimating achromat (L2). After L2, the signal passes through a planoconvex singlet (L3) and is recollimated by a second achromat (L4) at the rear of the ten-inch manipulator (TIM) that houses the telescope. The signal is then relayed toward a dichroic mirror that reflects the 532-nm probe beam. The self-emission passes through the dichroic mirror toward the SOP diagnostic shown in Fig. 138.23(b). Details of the optical telescope and the VISAR design can be found in Ref. 10.

The entrance to the SOP cabinet is an OG590 long-pass filter that transmits only light with a wavelength greater than 590 nm. Inside, the target emission is imaged onto the external slit of a Rochester Optical Streak System[12] (ROSS) camera by a series of periscopes and turning mirrors. A dove prism is used to rotate the target image on the slit, making it possible for the SOP to spatially resolve along any orientation on the target. To compensate for the refractive optics in the telescope (optimized for the 532-nm VISAR probe beam), the signal passes through a 300-mm planoconvex singlet (L5) and a 200-mm planoconcave singlet (L6) to focus the light onto the ROSS camera's external slit. Ahead of the slit are a second OG590 filter and any neutral density (ND) filters used for the experiment.

Inside the ROSS camera [bottom of Fig. 138.23(b)], the self-emission signal is focused by an Offner triplet system (M1–M3) onto the S20 photocathode with a sapphire window. Photoelectrons are accelerated through the streak tube toward

the phosphor screen. Photons emitted by the phosphor screen are transmitted through a 1:1 fiber-optic taper directly onto the charged-coupled–device (CCD) camera. The CCD is regularly binned 2 × 2 for an 1100 × 1100-pixel output. The data are spatially resolved in one dimension (along the slit length) and "streaked" in the other dimension to provide temporal resolution transverse to the slit. Data are recorded using 6-, 17-, 46-, or 96-ns sweep windows. The spectral range of the SOP (~590 to 850 nm) is defined by the OG590 filters at shorter wavelengths and the photocathode's insensitivity to infrared wavelengths.

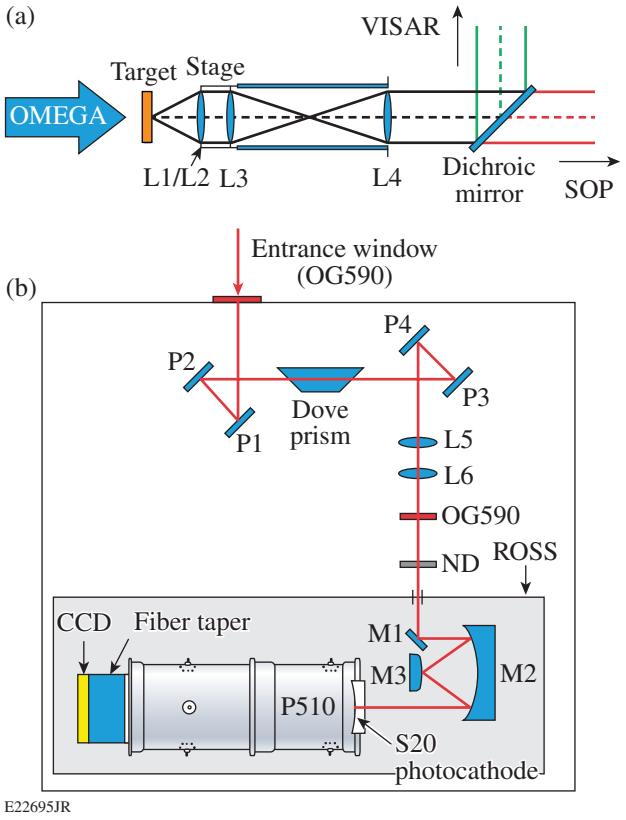

Figure 138.23
(a) OMEGA drivers launch a forward-moving shock wave through the target. The reflected VISAR (velocity interferometer for any reflector) probe beam and the self-emission of the material directly behind the shock front are simultaneously relayed outside the target chamber by the *f*/3.3 telescope. The 532-nm probe beam is reflected off the dichroic mirror and self-emission in the near-infrared passes through to (b) the SOP (streaked optical pyrometer) diagnostic. Self-emission enters the SOP diagnostic through an OG590 long-pass filter and is relayed by the SOP optics to the external slit of the Rochester Optical Streak System (ROSS) camera. The image of the slit is focused onto the S20 photocathode in the P510 streak tube by an Offner triplet, a 1:1 all-reflective image relay. Photons emitted by the phosphor screen are transmitted through a fiber-optic taper directly onto the charged-coupled–device (CCD) camera.

In 2011 the SOP was upgraded from the version described in Ref. 11 to that described above.[13] Most notably, the detector was upgraded from a Hamamatsu C4187 streak camera[14] to a ROSS camera.[12,15] The new streak camera contains a Photonis P510 streak tube[16] and an SI-800 TE cooled CCD camera[17] with an E2V CCD chip.[18] In addition, enhancements were made to the SOP optical relay.[13] These upgrades required an absolute calibration of the new system. The calibration method was similar to that of the previous SOP system as described in Ref. 11.

Calibration Method

The SOP was absolutely calibrated using a light source with a known spectral radiance: an Optronic Laboratories (OL550) Standard of Spectral Radiance, which is a modified GE Type 18A/T10/2P lamp having a tungsten ribbon filament fitted with a sapphire window.[19] This lamp, driven by a constant-current (15-A) power supply, has a National Institute of Standards and Technology (NIST)–traceable calibrated spectral radiance that is accurate to 1% (Ref. 19). The lamp was placed at the center of the OMEGA target chamber, and the telescope was adjusted until the tungsten ribbon filament was imaged onto the external slit of the SOP ROSS. Care was taken to ensure that the filament image was centered on the photocathode. Prior to the calibration, the photocathode's spatial profile was measured by scanning the external slit image across the photocathode by tilting the secondary mirror [M3 in Fig. 138.23(b)] of the Offner triplet system within the ROSS camera. The center and full width at half maximum (FWHM) of the photocathode were determined using the measured profile. These procedures ensured that the internal optics of the streak camera, which are motorized and adjusted remotely, were aligned consistently during calibrations and experiments.

During the calibration, the SOP was operated with a 5-s sweep window to produce sufficient intensity for the detector since the spectral radiance of the lamp ($T \sim 0.24$ eV) is considerably lower than that of a shock ($T > 1$ eV). To calibrate the spectral system response function of the SOP, seven 40-nm-wide bandpass filters were individually inserted to isolate narrow regions of the lamp's emission spectrum. The spectral system response of the SOP was determined by correcting an estimated response function using these narrowband measurements.

The SOP camera output in analog-to-digital units (ADU's) of a single pixel is given by

$$I = \frac{\Delta t}{G} \int_{\text{all } \lambda} \mathrm{d}\lambda \Phi_s(\lambda) T_x(\lambda) \mathrm{SR}(\lambda), \quad (1)$$

where Δt is the dwell time of a single pixel, G is the streak camera gain of photoelectrons to ADU's, $\Phi_s(\lambda)$ is the spectral radiant power from the light source, $T_x(\lambda)$ is the transmission of any removable ND or bandpass filters introduced to the system, and $SR(\lambda)$ is the SOP's spectral system response. The system response includes the S20 photocathode sensitivity and the transmission of all optical elements comprising the SOP. The transmission spectra of the ND and bandpass filters were measured using a Perkin-Elmer Lambda 900 spectrometer to 0.1% accuracy.[20] The dwell time,

$$\Delta t = \frac{W_{\mathrm{LSF}}}{B\Delta x \eta}, \tag{2}$$

is the amount of time that a given "streak" spends at a single pixel. B is the binning of the CCD (e.g., two for 2 × 2 binning), Δx is the length of one (square) pixel, η is the sweep rate given in pixels/ns, and W_{LSF} is the apparent slit width defined as the FWHM of the streak camera's line spread function (LSF). The ROSS camera optics provide a virtual cathode, resulting in an apparent external slit width that is considerably narrower than the actual slit width [Fig. 138.24(a)], enabling higher temporal resolution.

The spectral radiant power from the lamp's filament that maps to a single pixel is given by

$$\Phi_s(\lambda) = \int_{A_{\mathrm{pixel}}} \mathrm{d}A \int_{\Omega_{\mathrm{lens}}} \mathrm{d}\Omega L_s(\lambda), \tag{3}$$

where $L_s(\lambda)$ is the source radiance, A_{pixel} is the filament area that maps to a single pixel, and Ω_{lens} is the solid angle of the f/3.3 telescope. The amount of light that is recorded onto one pixel originates from a portion of the tungsten filament with the area

$$A_{\mathrm{pixel}} = \left(\frac{B\Delta x}{MM_{\mathrm{EO}}}\right)\left(\frac{B\Delta x W_s}{MW_{\mathrm{LSF}}}\right), \tag{4}$$

where W_s is the external slit width, M is the magnification from the light source to the photocathode, and M_{EO} is the magnification in the spatial direction (along the slit) of the electron optics within the streak tube.

An estimate for the wideband (590- to 850-nm) system response function was developed by combining the estimated sensitivity of the S20 photocathode and the measured transmission spectra of the SOP optics. This estimate was corrected using data taken in seven narrow wavelength regions using 40-nm-wide bandpass filters. Neutral-density (ND) filters were used as needed to limit the photocathode current. A series of three to five streaks were acquired with each bandpass filter in place, and the average of their measured intensities defined the SOP response in that wavelength range. For each of the seven wavelength ranges, the theoretical camera output I in ADU's was modeled using Eqs. (1)–(4) as

$$I = \frac{B\Delta x \Omega_{\mathrm{lens}} W_s}{GM^2 M_{\mathrm{EO}} \eta} \int_{\text{all } \lambda} \mathrm{d}\lambda L_s(\lambda) T_x(\lambda) \mathrm{SR}(\lambda) \tag{5}$$

with the estimate for $SR(\lambda)$ and the measured transmission spectra $T_x(\lambda)$ of the relevant bandpass and ND filters. The estimated system response was iteratively corrected until the model predicted the measured camera output in the seven narrowband regions. The validity of the corrected system response function was verified by calculating the camera output when observing the tungsten-filament source over the entire wavelength range of the SOP. The model correctly predicted the wideband measurements within 4%. The dashed line in Fig. 138.25 shows the calibrated spectral system response, and the solid line shows the spectral radiance of the calibrated tungsten-filament lamp over the SOP's wavelength range. The lamp's spectral radiance is NIST traceable and is characteristic of a 0.239-eV gray body with an emissivity of 0.215 (Ref. 19).

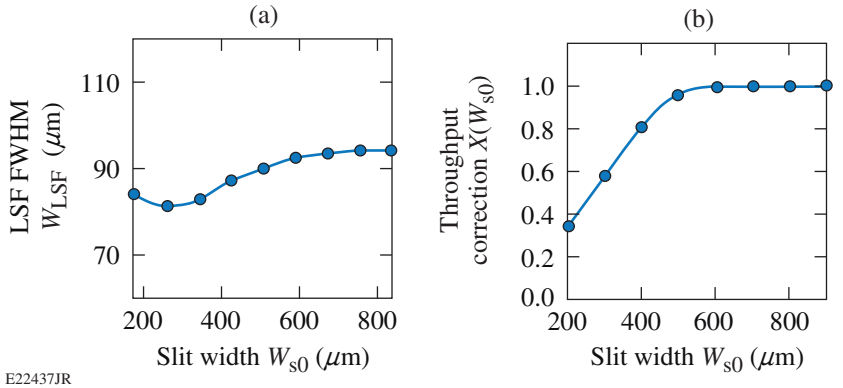

Figure 138.24
(a) The line spread function (LSF) full width at half maximum (FWHM) and (b) throughput correction vary with slit width. (a) The apparent slit width (W_{LSF}) is narrower than the actual slit width (W_{s0}) and remains fairly constant close to 90 μm for all slit widths. (b) Throughput correction [$X(W_{s0})$] in Eq. (8) is defined as the ratio of camera output at the experimental slit width (W_{s0}) to camera output at the calibration slit width (W_s) of 800 μm.

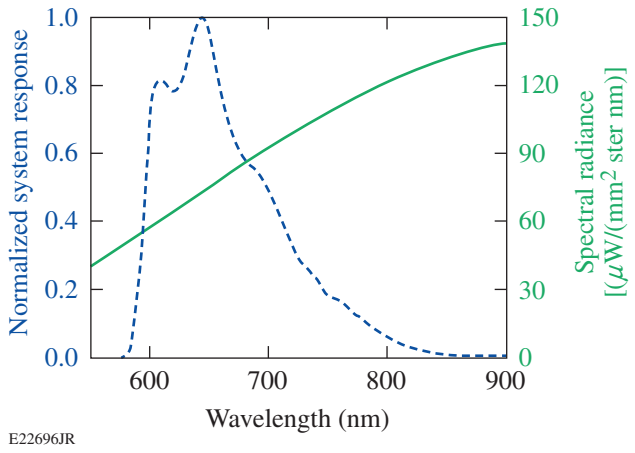

Figure 138.25
The SOP system response (dashed line) was determined using the individual spectral responses measured in each narrow wavelength region. A NIST–traceable tungsten-filament lamp with known spectral radiance (solid line) was used as the calibrated light source for the SOP calibration.

Brightness temperature is inferred from the SOP camera output by relating the spectral radiance $L_s(\lambda)$ of the observed source to that of an equivalent blackbody through Planck's law. The predicted SOP signal for such a source is given by

$$I = \frac{B\Delta x \Omega_{\text{lens}} W_s X(W_{s0}) 2hc^2}{GM^2 M_{EO}\eta} \int_{\text{all }\lambda} d\lambda \frac{T_x(\lambda)\text{SR}(\lambda)}{\lambda^5\left[\exp\left(\frac{hc}{\lambda T}\right)-1\right]}, \quad (6)$$

where h is Planck's constant, c is the speed of light, and $X(W_{s0})$ is the throughput correction defined as the ratio of the camera throughput at the experimental slit width W_{s0} to the camera throughput at the calibration slit width W_s. There is a nonlinear relationship between throughput and slit width as shown in Fig. 138.24(b). Since SR(λ) was determined at W_s and not necessarily W_{s0}, $X(W_{s0})$ adjusts for the difference in throughput. The throughput corrections for the slit widths of 200 to 800 μm are presented in Table 138.V. The adjustable parameters for an experiment include the experimental slit width W_{s0}, the sweep rate η, and the transmission spectra of the ND filters $T_x(\lambda)$. The first two parameters change the effective sensitivity of the camera for all wavelengths, whereas $T_x(\lambda)$ can have wavelength dependence and, therefore, must be included within the integral in Eq. (6). For a given experimental configuration [i.e., W_{s0}, η, and $T_x(\lambda)$], the camera output is calculated for a range of temperatures using Eq. (6). By approximating the wavelength dependence of the SOP as a δ function at the centroid wavelength of the integrand in Eq. (6), the predicted T versus I data are then fit to the relationship

$$T = \frac{T_0}{\ln\left(1+\frac{A}{I}\right)}, \quad (7)$$

where A and T_0 are calibration parameters determined by a least-squares fit. This approximation is valid since the spectral band of the SOP is narrow compared to the spectral band of a Planckian source with a temperature above 5000 K. Parameter A can be rewritten as

$$A = \frac{A_0 X(W_{s0})}{\eta}. \quad (8)$$

The system gain and binning ($B = 2$ for 1100 × 1100-pixel output) are fixed for all shots and are included in the calibration parameter A_0. Seven independent calibrations were performed to provide calibration parameters for SOP experiments beginning with shot 68276. The calibration parameters A_0 and T_0 (Table 138.VI) depend only on the shot number and ND filter used. There was an increase in the internal voltages of the streak camera that increased the values of A_0 beginning with shot 71573. There was also a subsequent decrease in SOP output caused by the accumulation of debris on the rear window of the TIM that houses the telescope. Because of these two effects, the values for A_0 must be scaled by the amounts specified in Table 138.VI for shots 71573 to 72436. Calibration parameter A_0 can be taken directly from Table 138.VI for shots 68276 to 71552 and shots 72437 to present.

To calculate brightness temperature from camera output in ADU's, one must first find the appropriate calibration parameters A_0 and T_0 from Table 138.VI; then use A_0 to calculate parameter A from Eq. (8) and both A and T_0 to calculate

Table 138.V: Throughput correction as a function of experimental slit width $X(W_{s0})$. There are two sets of values for the throughput correction because of a change in the external slit mechanism that occurred between shots 70551 and 70552. The throughput correction for shots 70552 and later is plotted in Fig. 138.24(b).

Experimental slit width W_{s0} (μm)	200	300	400	500	600	700	800
Shot 68276 to 70551	0.400	0.529	0.731	0.910	—	—	—
Shot 70552 to present	0.354	0.587	0.811	0.959	0.996	0.999	1.000

Table 138.VI: Brightness temperature is calculated using calibration parameters A_0 and T_0 in Eqs. (7) and (8). The calibration parameters are specified depending on the shot number and ND filter used in the experiment. ND filters are specified by their optical densities ranging from 0.1 to 2.5. For shots 71573 to 71875 multiply A_0 by 1.09. For shots 71876 to 72436 multiply A_0 by 1.05.

ND	T_0 (eV)	A_0 = ADU/ns
0	1.911	403,740
0.1	1.913	332,310
0.15	1.914	281,030
0.2	1.910	257,770
0.3	1.910	204,550
0.4	1.909	163,800
0.5	1.912	121,840
0.6	1.912	93,097
0.7	1.911	79,434
0.9	1.898	51,987
1.0	1.870	48,363
1.3	1.854	26,062
1.5	1.844	17,091
2.0	1.818	6,521
2.5	1.790	2,497

brightness temperature from Eq. (7). An example of inferred brightness temperature from SOP camera output for a typical experiment is shown in Fig. 138.26.

For experiments where a gray-body approximation is applicable, the intensity I is replaced by I/ε, where ε is the emissivity. Following Kirchoff's law for a body in thermal equilibrium,[6] the emissivity is equal to the absorptivity, i.e., $\varepsilon = 1-R$, where R is the reflectivity. If the dynamically compressed material is optically thick and reflects the 532-nm VISAR probe beam, one can extract R from the VISAR data. Temperatures for a gray body are then calculated using

$$T = \frac{T_0}{\ln\left[1 + \dfrac{(1-R)A}{I}\right]}. \tag{9}$$

VISAR/SOP Example

Gray-body temperatures were inferred from the SOP and the VISAR data obtained in experiments designed to study the EOS of quartz. These experiments used unsupported shocks that slowly decayed as they traversed the sample. Since the

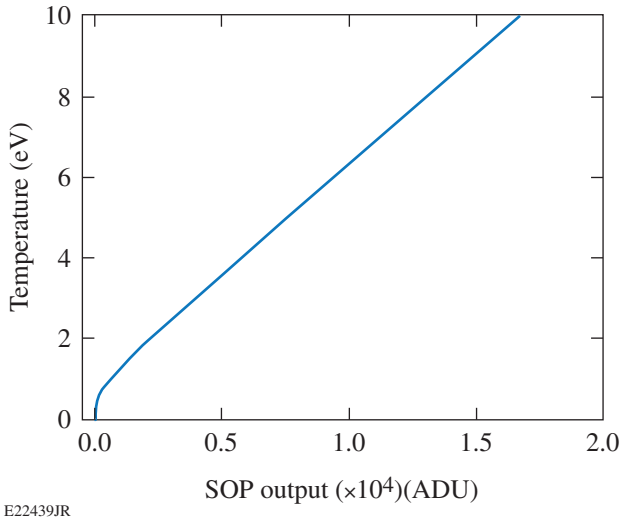

Figure 138.26
Inferred temperature dependence of the SOP signal for an experiment using a 17-ns sweep window, W_{s0} = 800 μm, and ND 0.3. This curve was generated using Eq. (7) with calibration constants A_0 = 204550 ADU/ns and T_0 = 1.910 eV calculated for data taken with an ND 0.3 filter.

α-quartz target samples were transparent, VISAR recorded the shock velocity and reflectivity of the decaying shock front as a function of time [Fig. 138.27(a)], while the SOP simultaneously recorded the self-emission intensity [Fig 138.27(b)]. The emission of the α-quartz sample at each time was converted to a gray-body temperature using Eq. (9) with the appropriate calibration parameters A and T_0 and the reflectivity inferred from VISAR. This temperature is plotted versus the VISAR velocity at that time [solid blue line in Fig. 138.27(c)], providing temperature versus shock velocity (pressure). These data are compared to a power law fit for temperature as a function of shock velocity in α quartz [dashed red line in Fig. 138.27(c)]. The power law fit was created using α-quartz data obtained by Hicks[5] and has the form $T = 1400 + 4.3\,U_s^{2.98}$, where U_s is the shock velocity in km/s and T is the temperature in Kelvin.

Error Analysis

A Monte Carlo routine was used to estimate the errors in this calibration method. Contributions include uncertainties in the filter transmissions T_x (0.1%), spectral radiance of the lamp L_s (1%), calibration slit width W_s (1%), sweep rate η (0.5% for slow sweeps used in calibrations and 2% for fast sweeps used in experiments), gain G (2%), throughput correction $X(W_{s0})$ (0.5% for an 800-μm-wide slit), and magnifications M (0.2%) and M_{EO} (0.5%). Uncertainties of 4% in parameter A_0 and 0.1% in parameter T_0 were estimated using 10,000 Monte Carlo runs that mimicked the calibration procedure and used the uncertainties in the narrowband measurements from the seven

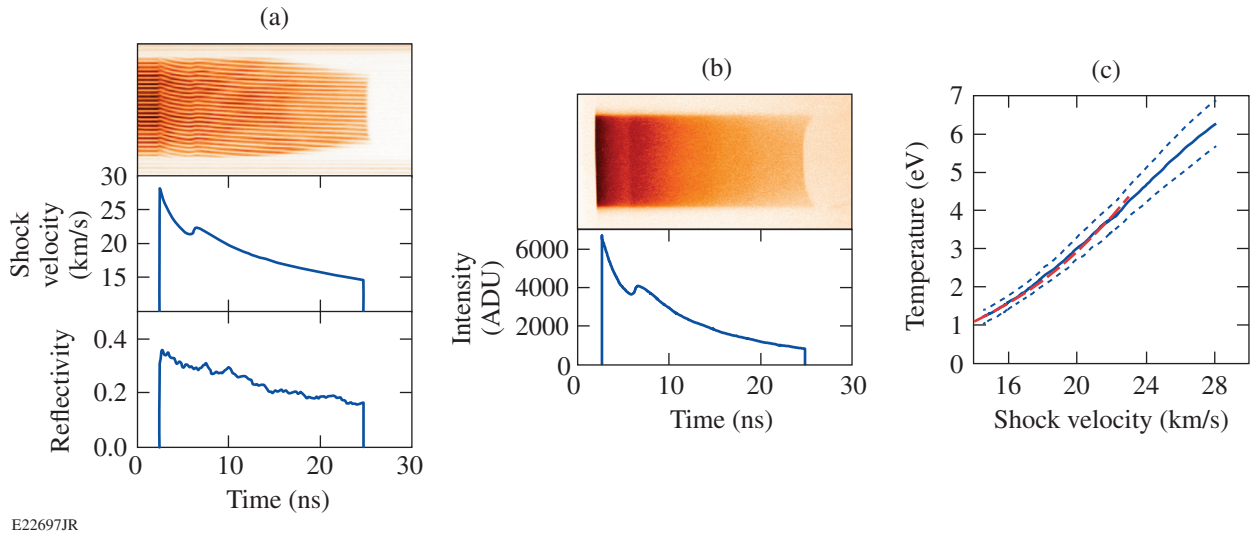

Figure 138.27
Sample VISAR and SOP data for an experiment using decaying shock waves in α-quartz targets for equation-of-state (EOS) studies. (a) The VISAR records temporally resolved shock velocity and reflectivity and (b) the SOP simultaneously records temporally resolved self-emission intensity. (c) Gray-body temperatures (solid blue line) were inferred from the SOP self-emission intensities using the SOP calibration and the VISAR reflectivity. The one-sigma standard deviations in temperature are represented by the dotted blue lines. These data are compared to a power law fit for temperature as a function of shock velocity in α quartz (dashed red line), which was created using α-quartz data obtained by D. Hicks (Ref. 5).

independent calibrations. For each routine, all parameters were varied within their error estimates, which produced 10,000 possible system responses, A_0's and T_0's. The narrowband responses measured in five of the calibrations agreed within 3%. The other two calibrations yielded narrowband intensities that were 9% and 5% higher as a result of the initial increase in streak camera voltages and the subsequent accumulation of debris on the rear window of the TIM. These two calibrations reflect the state of the diagnostic during shots 71573 to 72436 where the additional scaling of parameter A_0 is required. The estimated uncertainty of 4% for parameter A_0 is still valid for these shots, provided that the appropriate scaling specified by Table 138.VI is used.

The uncertainty in temperature for the data presented in Fig. 138.27(c) was 10.5% between 2 and 6 eV and increased to 14% at 1.2 eV. The SOP intensity data for this shot were particularly noisy in the low-intensity region, which resulted in 25% uncertainty in the lower intensities. This led to a larger uncertainty (~14%) in temperatures below 2 eV. A typical experiment with a 7% uncertainty in intensity, 4% uncertainty in A_0, 2% uncertainty in η, 0.5% uncertainty in $X(W_{s0})$, and 0.1% uncertainty in T_0 generates a total uncertainty in brightness temperature of 6.8% at 5 eV. This same experiment with a 20% uncertainty in reflectivity gives a 10% uncertainty in gray-body temperature at 5 eV.

Discussion and Conclusions

The streaked optical pyrometer on the OMEGA Laser System was absolutely calibrated using a NIST-traceable tungsten-filament lamp. Brightness temperatures of dynamically compressed materials are inferred from self-emission intensities using the spectral system response determined by the calibration. Gray-body temperature is calculated using the emissivity of the shock front determined by the VISAR measurement of its reflectivity.

Characterization of the streak camera throughput and LSF (Fig. 138.24) led to a recommendation of an 800-μm-wide slit for maximum throughput while maintaining temporal performance and providing some insensitivity to minor misalignments. Electron optics within the streak tube produce a virtual cathode, resulting in an apparent slit width that is considerably narrower than the actual slit width. The FWHM of the LSF (always <100 μm) is ~8.5× narrower than the actual slit width at 800 μm when the focus voltage of the streak tube is optimized for that slit width. When using the standard 2 × 2 binning for 1100 × 1100-pixel output and an 800-μm-wide slit, the temporal integration time is 155 ps for the 46-ns sweep window and 60 ps for the 17-ns sweep window. During experiments and calibrations, the image of the external slit is aligned to the center of the photocathode. The photocathode has varying sensitivity across its profile; therefore, narrow slit widths

are sensitive to alignment. Wide slit widths [i.e., greater than the FWHM of the photocathode (~550 μm)] are recommended to mitigate any slight misalignments, thereby minimizing shot-to-shot variations in camera performance. Uncertainty in the throughput correction [Fig. 138.24(b)] caused by a slight misalignment or inconsistency in the slit width is much lower for wide external slits. Uncertainty in $X(W_{s0})$ is 0.5% for slits greater than 600 μm and increases to 5% for narrow slit widths less than 600 μm. For these reasons, an 800-μm slit is recommended as a balance that optimizes throughput and temporal resolution while minimizing sensitivity to minor misalignment to the photocathode. The SOP calibration is performed using an 800-μm-wide slit.

To obtain brightness temperature from SOP intensity, one must first obtain the appropriate calibration constants A_0 and T_0 from Table 138.VI based on the ND filter used in the experiment. One then calculates parameter A from A_0 and the adjustable system parameters η and W_{s0} using Eq. (8). After acquiring A and T_0, one uses Eq. (7) to calculate brightness temperature or Eq. (9) to calculate gray-body temperature.

ACKNOWLEDGMENT

This material is based upon work supported by the Department of Energy National Nuclear Security Administration under Award Number DE-NA0001944, the University of Rochester, and the New York State Energy Research and Development Authority. The support of DOE does not constitute an endorsement by DOE of the views expressed in this article. We acknowledge R. Paguio, M. Farrell, and A. Nikroo (General Atomics) as well as D. R. Harding and M. J. Bonino for target preparation.

REFERENCES

1. J. D. Lindl, *Inertial Confinement Fusion: The Quest for Ignition and Energy Gain Using Indirect Drive* (Springer-Verlag, New York, 1998).
2. S. Hamel, L. X. Benedict, P. M. Celliers, M. A. Barrios, T. R. Boehly, G. W. Collins, T. Döppner, J. H. Eggert, D. R. Farley, D. G. Hicks, J. L. Kline, A. Lazicki, S. LePape, A. J. Mackinnon, J. D. Moody, H. F. Robey, E. Schwegler, and P. A. Sterne, Phys. Rev. B **86**, 094113 (2012).
3. R. P. Drake, *High-Energy-Density Physics: Fundamentals, Inertial Fusion, and Experimental Astrophysics*, Shock Wave and High Pressure Phenomena (Springer, Berlin, 2006).
4. A. Sawaoka, ed. *Shock Waves in Materials Science* (Springer-Verlag, Tokyo, 1993).
5. D. G. Hicks, T. R. Boehly, J. H. Eggert, J. E. Miller, P. M. Celliers, and G. W. Collins, Phys. Rev. Lett. **97**, 025502 (2006).
6. Ya. B. Zel'dovich and Yu. P. Raĭzer, in *Physics of Shock Waves and High-Temperature Hydrodynamic Phenomena,* edited by W. D. Hayes and R. F. Probstein (Dover Publications, Mineola, NY, 2002).
7. M. A. Barrios, D. G. Hicks, T. R. Boehly, D. E. Fratanduono, J. H. Eggert, P. M. Celliers, G. W. Collins, and D. D. Meyerhofer, Phys. Plasmas **17**, 056307 (2010).
8. J. H. Eggert, D. G. Hicks, P. M. Celliers, D. K. Bradley, R. S. McWilliams, R. Jeanloz, J. E. Miller, T. R. Boehly, and G. W. Collins, Nature Phys. **6**, 40 (2010).
9. T. R. Boehly, D. L. Brown, R. S. Craxton, R. L. Keck, J. P. Knauer, J. H. Kelly, T. J. Kessler, S. A. Kumpan, S. J. Loucks, S. A. Letzring, F. J. Marshall, R. L. McCrory, S. F. B. Morse, W. Seka, J. M. Soures, and C. P. Verdon, Opt. Commun. **133**, 495 (1997).
10. P. M. Celliers, D. K. Bradley, G. W. Collins, D. G. Hicks, T. R. Boehly, and W. J. Armstrong, Rev. Sci. Instrum. **75**, 4916 (2004).
11. J. E. Miller, T. R. Boehly, A. Melchior, D. D. Meyerhofer, P. M. Celliers, J. H. Eggert, D. G. Hicks, C. M. Sorce, J. A. Oertel, and P. M. Emmel, Rev. Sci. Instrum. **78**, 034903 (2007).
12. P. A. Jaanimagi, R. Boni, D. Butler, S. Ghosh, W. R. Donaldson, and R. L. Keck, in *26th International Congress on High-Speed Photography and Photonics*, edited by D. L. Paisley *et al.* (SPIE, Bellingham, WA, 2005), Vol. 5580, pp. 408–415.
13. *November 2011 Progress Report on the Laboratory for Laser Energetics, Inertial Confinement Fusion Program Activities*, University of Rochester, Rochester, NY (2011).
14. Framing Streak Camera C4187, *Hamamatsu Specification Manual*, Hamamatsu Photonics K.K., Electron Tube Center, Japan.
15. Sydor ROSS 5100 Specification Manual, Sydor Instruments, LLC, Rochester, NY 14624.
16. PHOTONIS P510 Streak Tube Specification Manual, PHOTONIS, 19106 Brive, France.
17. Spectral Instruments 800S CCD Camera Specification Manual, Spectral Instruments, Tucson, AZ 85745 (http://www.specinst.com/Products/800s_datasheet.pdf).
18. e2v technologies, Elmsford, NY 10523-1482.
19. *OL Series 550 Standards of Spectral Radiance with Sapphire Windows Specification Manual*, Optronic Laboratories, Inc., Orlando, FL 32811.
20. Lambda900 Spectrophotometer, PerkinElmer, Waltham, MA 02451.